Radiative and Microphysical Properties of Autumnal Arctic Clouds

J. O. Pinto and J. A. Curry
Program in Atmospheric and Oceanic Sciences
University of Colorado
Boulder, Colorado

Introduction

Clouds strongly modulate the surface energy budget over the Arctic ice pack. In autumn, as the amount of insolation rapidly decreases, their main influence is felt through enhancing the emissivity of the cold dry atmosphere. During autumn, low clouds are present over the arctic ice pack nearly 60% of the time. In addition, ice clouds, which are not included in this statistic, become increasingly common as autumn progresses. The microphysical properties of these clouds, which determine their radiative impact, are not well known due to the dearth of observations. A main objective of the Beaufort and Arctic Storms Experiment (BASE) was to document and understand the transition in cloud properties over the Arctic ice pack in autumn from predominantly liquid to crystalline.

BASE consisted of 14 research flights of the National Center for Atmospheric Research's (NCAR) C-130 during a 5-week period beginning 21 September 1994. The flights were conducted within the domain shown in Figure 1, with many missions flown over the multiyear ice pack which covered much of the Beaufort Sea except north of the southern coast. Details of the experiment and the suite of instrumentation on board the NCAR C-130 are given in Curry et al. (1997) and Pinto (1997).

During BASE, a total of 50 individual cloud decks were observed at various heights in the atmosphere. For classification purposes, each cloud layer in multiple-layer cloud systems has been counted separately. Of the 50 cloud layers observed, 20 had tops below 2.5 km (low), 10 were considered to be mid-level clouds (i.e., top and base both between 2 and 5 km), and 8 were classified as high ice clouds (cloud top > 5 km). In this report, the microphysical and radiative properties of several low clouds of differing predominant particle phase are discussed.

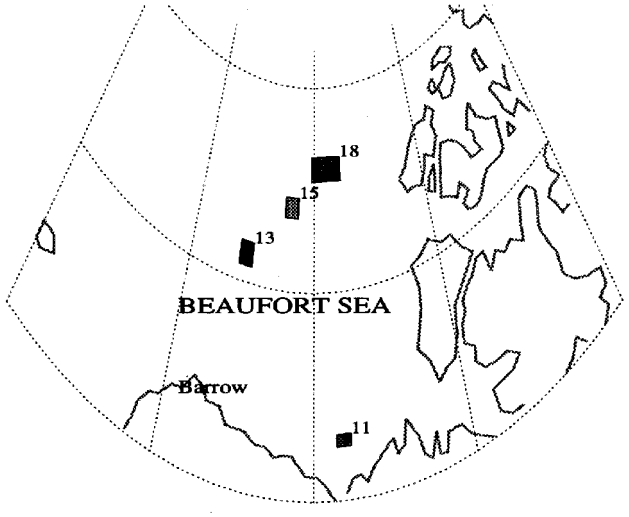

Figure 1. Beaufort Sea region over which BASE flight campaigns were conducted. Boxes denote regions where cloudy boundary layers were sampled and are annotated with their corresponding flight numbers.

Cloud Microphysical Analysis

The microphysics instrumentation on board the NCAR C-130 included the particle measuring system (PMS) 2DC and 2DP probes and the PMS Forward Scattering Spectrometer Probe (FSSP). The FSSP detected cloud particles ranging from 5-47 μm with a bin size of 3 μm. The 2DC probe sized particles from 25-800 μm in diameter with a resolution of 25 μm, and the 2DP probe sized particles ranging from 200-6400 μm with 200-μm resolution. Data collected by each of these instruments was combined to produce a composite particle size distribution. The aircraft also had a King Probe for measuring liquid water contents and a Rosemount icing Rate Detector for detecting the presence of supercooled liquid water. The data collected from all of the microphysics probes were used to determine the phase, size and amount of condensed water present in each cloud layer.

Liquid Cloud

Several low clouds were determined to be predominately liquid; although all of the low clouds observed during BASE contained at least some ice. The clouds are categorized as liquid if more than 98% of the condensed phase is liquid. Figure 2 depicts an example of a predominantly liquid cloud. Ice particle concentrations of less than 0.1 L^{-1} were detected with the 2DC probe in this particular cloud layer (not shown).

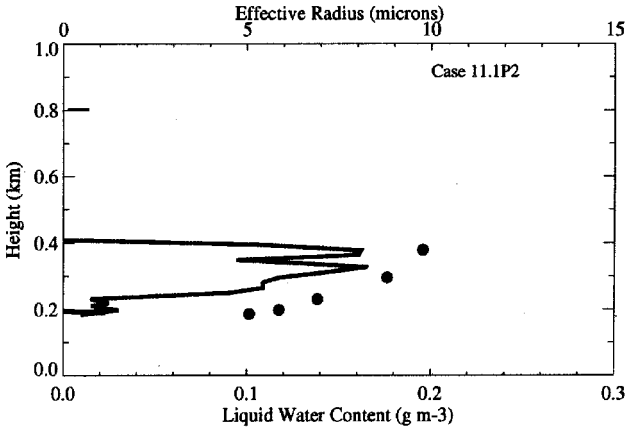

Figure 2. Profiles of LWC (line) and effective radius (closed circles) obtained during a vertical descent through a liquid cloud observed over the Beaufort Sea (Case 11). Effective radii are calculated from 5-s average FSSP size distributions. The LWC is obtained from a 1-s King Probe data.

The liquid cloud shown in Figure 2 was observed on 12 October 1995 at 2130 UTC over an open water region of the Beaufort Sea (Case 11). The cloud top height varied between 350-400 m, with a base of 200 m. The liquid water contents (LWC) are greater than would have been expected through adiabatic lifting, which is indicative of strong radiative cooling in the cloud layer. A liquid water path of 29.7 g m^{-2} is obtained from the observed LWC profile. For effective radius calculation, the cloud drop concentration in bin #1, which is missing from the data, is assumed to be equal to that in bin #2 (see Figure 3). This assumed concentration of 2-5 μm particles, which has been determined to be accurate to within +/- 10% based on previous cloud particle size distributions observed in Arctic stratus, is crucial for the

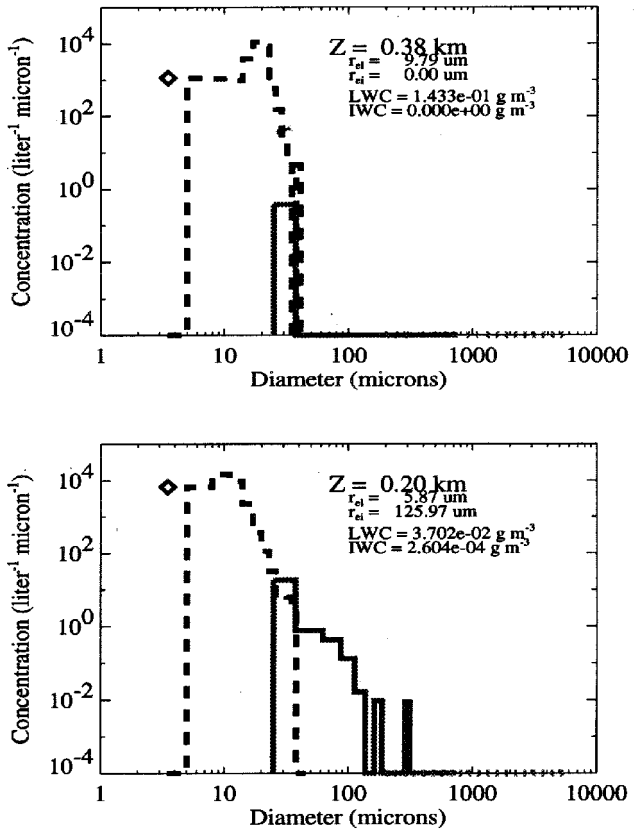

Figure 3. Composite cloud particle size distributions at two heights in a liquid cloud layer using 5-s averages during a vertical descent of the C-130. FSSP data represented with dashed line and 2DC with solid line. Diamond denotes assumed particle concentration for missing bin #1.

determination of the effective radius. The effective radius generally increases with height through the cloud layer, with a mean effective radius for the entire cloud deck of 7.3 μm.

More detailed microphysical information is revealed in the cloud particle size distributions (Figure 3). The size spectra at cloud top (0.38 km) are bimodal with peaks at 6.5 (not easily seen in figure) and 18.5 μm. No particles larger than 45 μm are observed at this level. At cloud base the spectra show a single broad peak at 9.5 μm, with large concentrations of small particles and an extended tail that is attributed to sedimentation of larger particles from some height within the cloud.

Mixed-Phase Cloud

In mixed-phase clouds, the FSSP, King Probe and Icing Probe detect liquid water; however, the FSSP-derived LWCs are significantly lower than those obtained with the other two probes. The composite spectra in mixed-phase clouds have two distinct properties: a pronounced narrow peak at the smallest FSSP sizes and evidence of a gap between the FSSP and the 2DC segments of the size distribution. Although the FSSP spectra indicate that smaller liquid drops are present in the cloud layer, an estimate of the mean liquid particle size cannot be made because of the noise introduced by the presence of ice crystals. In addition, the phase of cloud particles less than 100 μm in diameter cannot be determined due to a lack of resolution in the 2DC images. Using only those particles whose phase has been unambiguously determined results in a substantial overestimate of mean ice particle size in the cloud.

Because of the problems inherent in the determination of mean liquid and ice particle sizes in mixed-phase clouds, only profiles of liquid and ice water content (IWC) are reported (Figure 4). The data collected by the 2D probes were analyzed with software provided by the NCAR Research Applications Program (RAP) (George et al. 1995). The IWCs were determined as a function of particle diameter and aspect ratio using mass-diameter relationships similar to those used by McFarquhar and Heymsfield (1996). Only particles whose phase could be unambiguously determined (i.e., D > 100 μm) were included in the IWC determination. These estimated IWCs are fairly accurate since the smaller particles contain only a small fraction of the total ice mass.

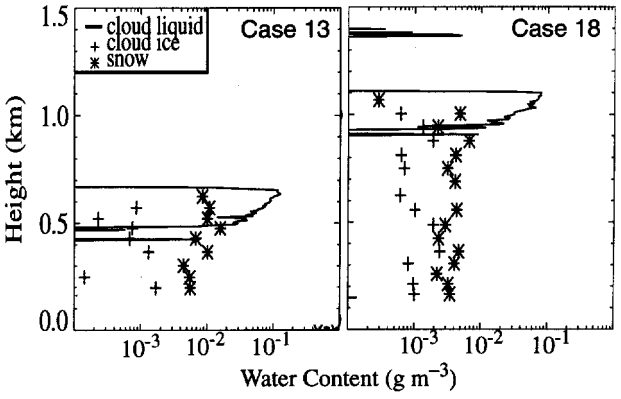

Figure 4. Profiles of liquid and IWC for two mixed-phase cloud layers observed during vertical transects by the C-130 over the Arctic ice pack. Solid lines indicate 1-s King Probe LWC. The pluses and asterisks indicate IWC derived from 10-s 2DC and 2DP probe measurements, respectively.

The two profiles shown are from cloud events observed over the multiyear ice pack on two different days (16, 25 October 1994—Case 13 and 18, respectively. The liquid water content measured in these mixed-phase clouds is considerably less than that found in the liquid cloud. The liquid water content increases with height toward cloud top, while IWC is fairly constant with height. The relative amount of ice in the cloud layer therefore increases toward cloud base. Precipitation in the form of snow is observed beneath both cloud decks. These precipitating, mixed-phase clouds were observed at temperatures between -20 and -13° C.

Composite particle size distributions are shown for two heights in the boundary layer of Case 13 (Figure 5). In the distribution obtained within the cloud layer (Figure 5a), there is a sharp decline in concentration where the FSSP and 2DC spectra intersect. This feature was often observed in the mixed-phase clouds. Also note the characteristic flat shape of the FSSP distribution at 0.11 km, indicating the presence of only ice particles. Large snow crystals are observed throughout with numerous particles exceeding 2.5 mm in diameter. A slight reduction in size of the snow particles and in the IWC toward the surface is evident and may be attributed to sublimation.

Ice Cloud

Boundary layer ice clouds observed from the NCAR C-130 appeared as sun pillars produced from the optical effect that the ice particles had on the incoming solar radiation at large solar zenith angles. This type of cloud is often termed "clear-sky ice crystal precipitation." During BASE, two ice clouds were observed in the boundary layer; however, only one case, which occurred on 19 October (Case 15), has been extensively analyzed due to problems with the data. These two boundary layer ice clouds were observed at temperatures between -19 and -12° C, similar to that observed in the mixed-phase clouds. In these pure ice clouds, the King and Icing Probes detect nothing. The FSSP detects the presence of cloud particles; however, these data were deemed to be unreliable because of the presence of large ice particles which are known to contaminate FSSP measurements.

The 2DC and 2DP probe data were analyzed in a method similar to that employed in the mixed-phase case. Ice water contents were obtained by integrating over diameters ranging from 25 to 3000 μm. The IWCs in Case 15 were determined using size distributions obtained from 2-minute averages from extended horizontal legs and from 10-s averages obtained during a vertical descent of the aircraft.

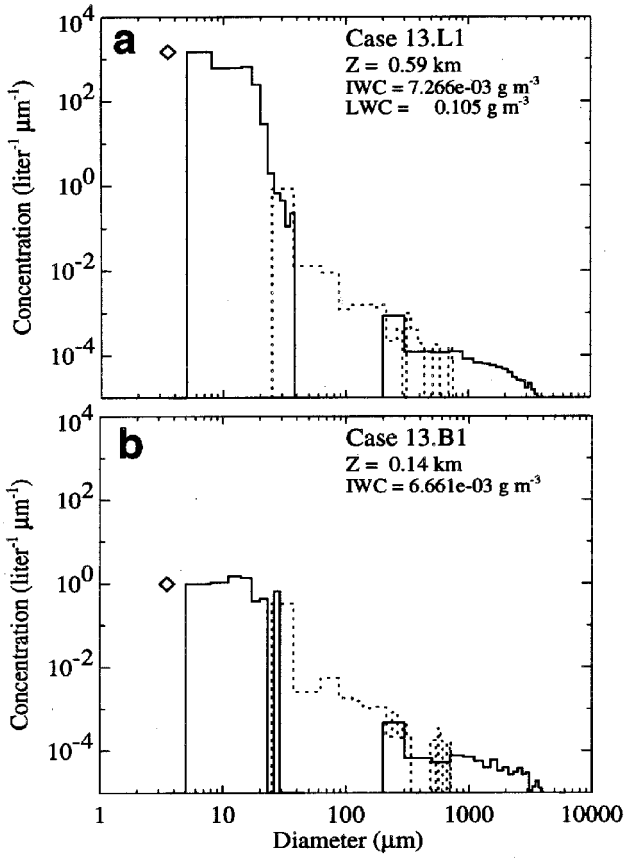

Figure 5. Composite size distributions obtained during two extended horizontal legs for Case 13 at (a) 0.59 km and (b) 0.14 km. The distributions are generated from 2-minute averages of FSSP (solid), 2DC (dotted) and 2DP (solid) data.

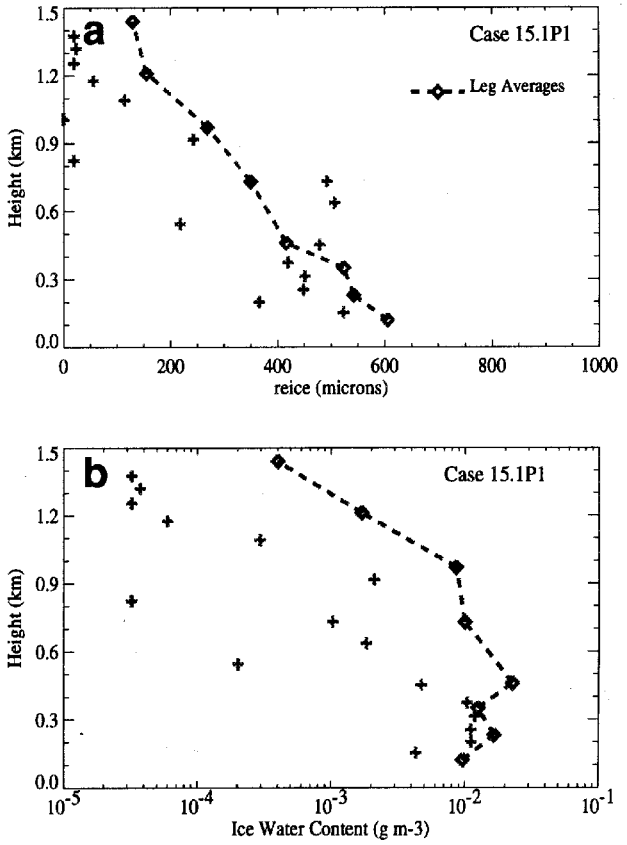

Figure 6. Profiles of (a) equivalent-sphere ice effective radius, reice, and (b) IWC obtained for the low-level ice cloud (Case 15). The pluses indicate 10-s averages obtained during a vertical descent while diamonds denote extended horizontal leg averages.

Profiles of IWC and equivalent-sphere effective radius are shown in Figure 6. The ice cloud is roughly 1.5-km deep, containing low concentrations of ice particles. The mean ice particle sizes and IWC increase toward the surface with a maximum IWC and effective radius of 0.025 g m^{-3} and 400-600 µm, respectively. Comparison of leg-average IWC to that obtained during long vertical descents reveals that the profile method significantly underestimates the IWC when IWCs are small.

Particle size distributions reveal the vertical structure in the microphysical properties of the cloud layer in more detail (Figure 7). Near cloud top the particles are less than 600 µm in diameter, and the distribution has a fairly steep slope beginning around 250 µm. At the lower levels the distribution flattens somewhat as particles greater than 1 mm diameter are detected. Some evidence of bimodality in the distribution exists, possibly indicative of coagulation of cloud ice particles forming snow. Near the surface, there are fewer large particles. Note that the FSSP distribution has that characteristic flat shape indicative of ice particles. The 2DC images reveal that the ice particles are generally irregular in shape.

Radiative Transfer

The radiative properties of the cloud layers are determined through aircraft observations obtained during extended horizontal legs and by using a two-stream radiative transfer model. Only longwave radiation is considered since only small amounts of solar radiation reach the Arctic this time of year. In addition, solar zenith angles are so large (e.g., >80°) that the plane-parallel approximation cannot be made as

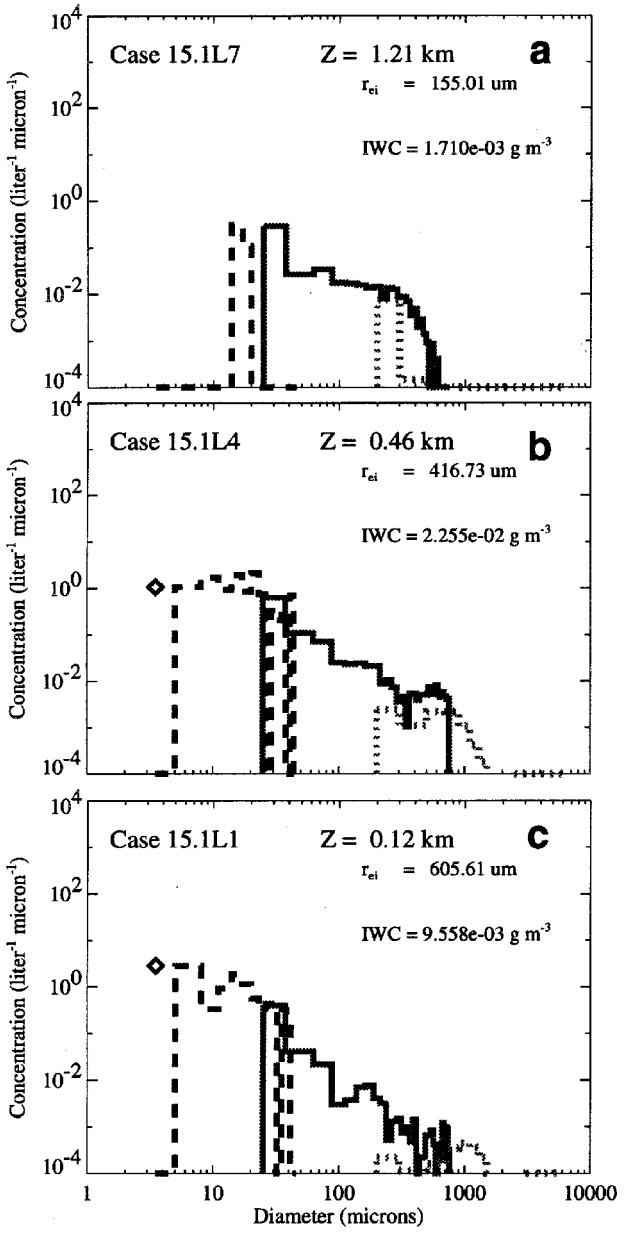

Figure 7. Composite size distributions obtained during three extended horizontal legs for Case 15 flown at (a) 1.21 km, (b) 0.46 and (c) 0.12 km. The distributions are generated from 2-minute averages of FSSP (dashed), 2DC (solid) and 2DP (dotted) data.

solar radiative transfer becomes a 3D problem. Leg average upward and downward longwave fluxes are obtained with Eppley pyrgeometers and are used to determine the emissivity of the cloud layer.

The two-stream model employed here was originally developed by Toon et al. (1990) and is now part of the Streamer modeling system (Key 1996). It includes gaseous absorption by CO_2, H_2O, O_3 and O_2 using 105 bands. The cloud properties are determined following Hu and Stamnes (1993) for liquid. A similar parameterization was developed for ice based on Mie scattering by spherical ice particles by Key (1996). A background profile of marine aerosols with an aerosol optical depth of 0.08; a standard sub-arctic ozone profile; and observed temperature, water vapor, and cloud microphysical profiles and observed surface temperature are used in the radiative transfer calculations. Since a liquid effective radius cannot be derived for the mixed-phase cloud, 7 μm is assumed while the calculated ice effective radii are used.

The observed and modeled downwelling longwave flux profiles shown in Figure 8 match fairly well; however, significant discrepancies in the upwelling flux in Cases 11 and 18 are noted. The fact that the downwelling fluxes match fairly well below cloud top is an indirect verification of the cloud microphysical measurements. The modeled upward fluxes differ from the observed values by as much as 10 W m^{-2} in the liquid case and 6 W m^{-2} in the mixed-phase case. Differences between the modeled and observed upward flux may be attributed to inaccurate specification of the surface boundary conditions due to horizontal inhomogeneities. The observed and modeled radiative flux profiles in the ice case match fairly well. A good deal of horizontal inhomogeneity in the cloud properties is evident in the large error bars in the observed downward flux.

The cloud emissivity may be determined from the observed fluxes obtained above and below the cloud deck and the observed temperature profile following Curry and Herman (1985). The cloud emissivities determined for the liquid, mixed-phase and ice clouds using this technique are 0.91, 0.8 and 0.2, respectively.

The net effect of the clouds on the downward flux at the surface may be determined using the radiative transfer model. The longwave "cloud forcing" may be calculated following $F_{cld} - F_{clr}$ where both F_{cld} and F_{clr} are determined with the radiative transfer model. It is found that the optically thin ice cloud increases the downward flux at the surface by just 5 W m^{-2} relative to clear-sky conditions. The mixed-phase cloud in Case 18 increases the downward longwave flux by 54 W m^{-2}. The liquid cloud increased the downward flux at the surface by 77 W m^{-2}.

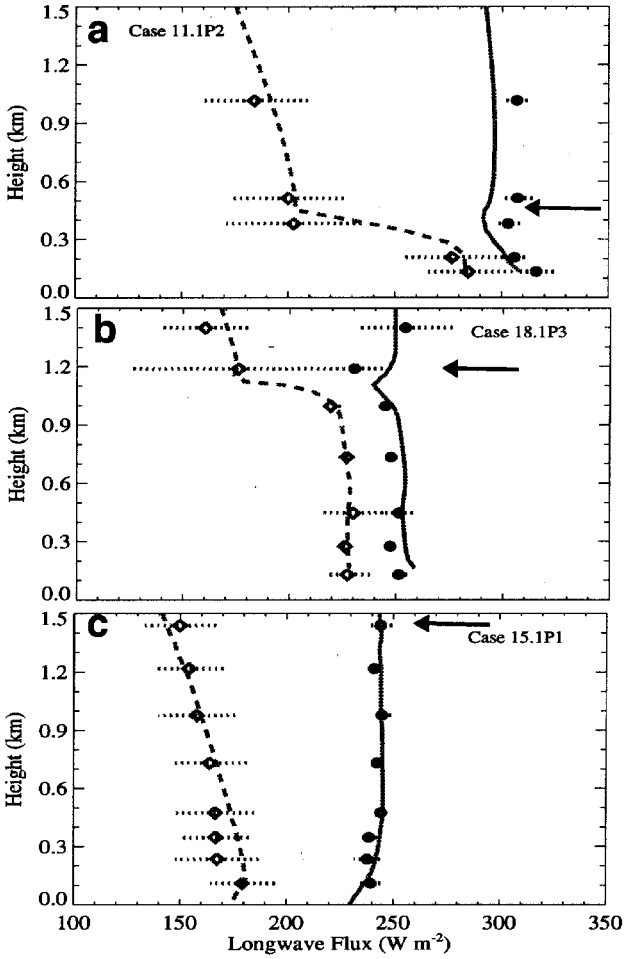

Figure 8. Upward and downward longwave radiative flux profiles obtained from leg averages (diamonds - downward, filled circles - upward) and from a radiation model (dashed lines - downward, solid lines - upward) for (a) liquid cloud, (b) mixed-phase cloud and (c) ice cloud. The dotted error bars denote two standard deviations in the observations. Arrows denote cloud top location.

Summary and Conclusions

The radiative and microphysical properties of low-level clouds of varying phase have been described. Although no clouds were completely free of ice particles, several contained very low concentrations of ice and were considered to be liquid clouds. A detailed description of low-level liquid, mixed-phase and ice clouds observed over the Arctic ice pack has been given. Several additional low-level clouds have been analyzed and the results are consistent with those presented here.

The relationship between the predominant cloud particle phase and in-cloud temperature is rather tenuous, as is seen in Figure 9. The temperatures observed in the two mixed-phase clouds are similar to those observed in the two pure ice clouds. The predominantly liquid cloud is seen to occur at much warmer temperatures. Additional observations are necessary to develop useful temperature phase relationships for low-level clouds. These types of relationships are necessary to improve the treatment of low clouds over Arctic ice pack in global climate models. Observations of atmospheric chemistry are also necessary to understand these relationships.

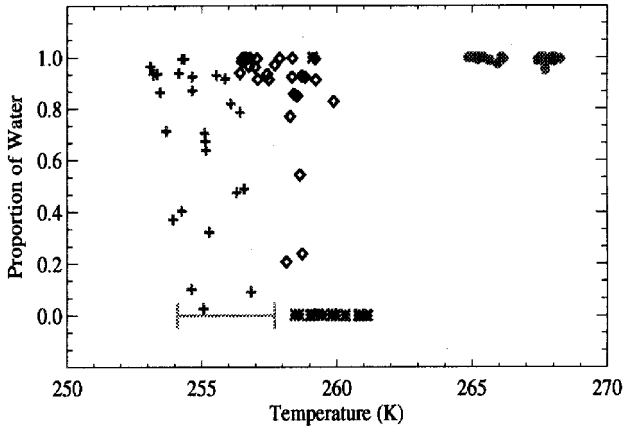

Figure 9. Ratio of liquid water to total condensed water mass (liquid + ice) observed during aircraft profiling through cloud layers. Symbols stand for different cloud events (i.e., error bar - ice [Case 17], pluses - mixed [Case 18], diamonds - mixed [Case 13], filled circles - liquid [Case 11], asterisks - ice [Case 15]).

The low clouds occurring in the Arctic are characterized by properties much different than those observed at lower latitudes. Mixed-phase clouds and ice clouds occur in the boundary layer, often within complex vertical temperature profiles. The mixture of liquid and ice makes determination of the mean particle size in mixed-phase clouds difficult, precluding an accurate description of the cloud's radiative properties.

The radiative properties of these clouds are quite different from that found at lower latitudes. In the three examples given

here, the cloud emissivity was less than unity, with emissivities decreasing as the proportion of cloud ice increased. The ice clouds are very thin optically despite filling an appreciable depth of the atmosphere. Although the ice case reported here produced only a 5 W m^{-2} increase in the downward longwave flux, these low-level ice clouds are thought to have a large effect on the downward longwave flux at the surface as temperature inversions strengthen as the Arctic night approaches (Curry et al. 1990). Ice crystal clouds are also instrumental in the radiative cooling to space of the Arctic atmosphere, enhancing formation of cold-core anticyclones.

References

Curry, J. A., and G. F. Herman, 1985: Infrared radiative properties of summertime arctic stratus clouds. *J. Clim. Appl. Meteor*., **24**, 526-538.

Curry, J. A., F. G. Meyer, L. F. Radke, C. A. Brook, and E. E. Ebert, 1990: Occurrence and characteristics of lower troposphere ice crystals in the Arctic. *Int. J. Climatol*., **10**, 749-764.

Curry, J. A., J. O. Pinto, T. Bennert, and M. Tschudi, 1997: Evolution of the cloud boundary layer during the autumnal freezing of the Beaufort Sea. *J. Geophys. Res*., in press.

George, J., A. Jones, and R. Vaughan, 1995: *2DANAL: User Documentation, Version 1.1*. National Center for Atmospheric Research, Boulder, Colorado.

Hu, X. Y., and K. Stamnes, 1993: An accurate parameterization of the radiative properties of water clouds suitable for use in climate models. *J. Clim.*, **6**, 728-742.

Key, J., 1996: *Streamer User's Guide*. Technical Report 96-01, Department of Geography, Boston University, Boston, Massachusetts.

McFarquhar, G. M., and A. J. Heymsfield, 1996: Microphysical characteristics of three anvils sampled during the Central Equatorial Pacific Experiment (CEPEX). *J. Atmos. Sci*., **53**, 2401-2423.

Pinto, J. O., 1997: Autumnal mixed-phase cloudy boundary layers in the Arctic. Submitted to *J. Atmos. Sci*.

Toon, O. B., C. P. McKay, and T. P. Ackerman, 1990: Rapid calculation of radiative heating rates and photodissociation rates in inhomogeneous multiple scattering atmospheres. *J. Geophys. Res*., **94**, 16287-16301.